World Academy of Science, Engineering and Technology
International Journal of Chemical and Molecular Engineering
Vol:16, No:9, 2022

Simulation of Complex-Shaped Particle Breakage Using the Discrete Element Method

Felix Platzer, Eric Fimbinger

Abstract—In Discrete Element Method (DEM) simulations, the breakage behavior of particles can be simulated based on different principles. In the case of large, complex-shaped particles that show various breakage patterns depending on the scenario leading to the failure and often only break locally instead of fracturing completely, some of these principles do not lead to realistic results. The reason for this is that in said cases, the methods in question, such as the Particle Replacement Method (PRM) or Voronoi Fracture, replace the initial particle (that is intended to break) into several sub-particles when certain breakage criteria are reached, such as exceeding the fracture energy. That is why those methods are commonly used for the simulation of materials that fracture completely instead of breaking locally. That being the case, when simulating local failure, it is advisable to pre-build the initial particle from sub-particles that are bonded together. The dimensions of these sub-particles consequently define the minimum size of the fracture results. This structure of bonded sub-particles enables the initial particle to break at the location of the highest local loads – due to the failure of the bonds in those areas – with several sub-particle clusters being the result of the fracture, which can again also break locally. In this project, different methods for the generation and calibration of complex-shaped particle conglomerates using bonded particle modeling (BPM) to enable the ability to depict more realistic fracture behavior were evaluated based on the example of filter cake. The method that proved suitable for this purpose and which furthermore allows efficient and realistic simulation of breakage behavior of complex-shaped particles applicable to industrial-sized simulations is presented in this paper.

Keywords—Bonded particle model (BPM), DEM, filter cake, particle breakage, particle fracture.

I. Introduction

DURING many industrial processes, the particles of bulk solids with various material properties and shapes are broken down into smaller fragments, which can further break again. In many cases, this breakage is undesirable, such as the degradation of sinter during conveyance of this bulk material to the blast furnace since too fine-grained particles impede a sufficient gas flow in the furnace [1], when exceeding the maximum load-bearing capacity of building materials, such as concrete, in the construction industry [2], [3], or the damage of supporting rock structures in mining engineering [4], [5]. However, there are also many areas in which material breakage is desired, such as relating to crushing, grinding or drilling rock in the areas of mining engineering and mineral processing [4], [6], [7], handling cemented sands or heavily overconsolidated soils [8], or the cutting and threshing of agriculture products during harvesting [9], [10], only to name a few.

Irrespective of whether the material failure is desired or not, using a well-calibrated and for the process that is intended to be depicted suitable numerical simulation, the breakage of a particle can be replicated very accurately in a simulation environment. This is particularly suitable for optimizing processes in a very time- and cost-efficient manner.

The project on which this paper investigates the fracture behavior of filter cakes [11], generated from a filter press in the shape of a relatively flat plate, during the conveying process using conveyor belts and a chute system. During the material transfer, the complex-shaped cake plates break abruptly and locally, which is to be simulated by means of a numerical simulation method (specifically the Discrete Element Method (DEM), correspondingly, as a particle-based system is present). Due to the rather low moisture content of the filter cake, this material setup exhibits brittle material failure after a relatively small initial elastic deformation. The goal of this paper is to depict the macroscopic breakage behavior of sample plates made of this type of filter cake material in a sufficient way, providing a way to numerically predict if and where such filter cake plates fracture in process-like situations. It is furthermore said that this approach is thus not intended to replicate the exact microscopic crack propagation in a single sample, as the focus is set on depicting effects from a bulk-oriented perspective. To depict filter cake breakage, the Discrete Element Method (DEM) [12], also called Distinct Element Method [13], is ideal since in many other methods the simulated material is considered as a homogeneous continuum, whereas in DEM it is represented as discrete and inhomogeneous [14], which is required for the case in question. In DEM software, the change of motion and position of particles between discrete timesteps is computed based on the forces and torques acting on said particles using the laws of motion. These forces can be divided into general forces ($F_{General}$), forces due to gravity or force fields, and contact forces ($F_{Contact}$) resulting from interactions of a particle with other particles or system components.

$$F_{Particle} = F_{Contact} + F_{General} \tag{1}$$

Furthermore, the contact force is divided into master contact force F_{Master} and slave force F_{Slave}, which will be superimposed by means of superposition.

F. Platzer is Chair of Mining Engineering and Mineral Economics-Conveying Technology and Design Methods, Montanuniversität Leoben (University of Leoben), FranzJosef-Strasse 18, 8700 Leoben, Austria (e-mail: felix.platzer@unileoben.ac.at).

E. Fimbinger is Chair of Chair of Mineral Processing, Montanuniversität Leoben (University of Leoben), FranzJosef-Strasse 18, 8700 Leoben, Austria (e-mail: eric.fimbinger@unileoben.ac.at).

$$F_{Contact} = F_{Master} + F_{Slave} \tag{2}$$

The master contact force corresponds to the sum of forces resulting from the basic contact model, or master contact model, in the normal and tangential direction of particles in contact (cf. [15]). Additionally added slave contact models can be added to represent various physical phenomena, such as cohesion acting between moist particles, or in this case: a physical connection of particles making up a continuum.

In this paper, the DEM-based Multiphysics simulation software ThreeParticle/CAE by BECKER3D [16] was used for simulation.

II. Bonded Particle Model

Of the various methods that can be used in DEM to represent particle breakage, the Bonded Particle Model (BPM) [8], [14], [17] is ideally suited to represent local material failure under preceding deformation. In this method, two discrete particles are joined together with a virtual connection called a bond, also known as a joint or bonding. This element has neither mass nor volume but exerts loads (forces/torques) on the two particles joined by a bond as they deviate from their original relative positions. If several sub-particles are bonded together to form a cluster, any complex particle shape, from this point on called the parent particle, can be represented as such a bonded particle network. A bond connection in its initial state and under deformation is depicted in Fig. 1.

In Three Particle, bonds are implemented as a slave contact model and can transmit tensile, compressive, and shear forces, as well as torque and bending moments. The forces are calculated in a local bond coordinate system with the x-axis corresponding to the bond axis, as seen in Fig. 1. For this reason, all quantities required for the calculation of the bond forces and moments, such as the strain Γ, the curvature of the bonds κ, the translational as well as relative rotational velocity v_{12} resp. Ω_{rel}, are expressed in local bond coordinates.

The reaction forces $F_{s,ax}$ are calculated from the Youngs Modulus E_b, the cross-section A_b, the shear coefficient α_s, and the shear modulus of the bond G_b, according to (3).

$$F_{s,ax} = \begin{bmatrix} E_b A_b & & \\ & \alpha_s G_b\ A_b & \\ & & \alpha_s G_b\ A_b \end{bmatrix} \Gamma \tag{3}$$

The viscous damping force F_d is then

$$F_d = d\ v_{12} \tag{4}$$

with the damping coefficient d. The torque acting between the bonded particles $T_{b,t}$ is calculated from

$$T_{b,t} = \begin{bmatrix} 2G_b\ J_b & & \\ & E_b J_b & \\ & & E_b J_b \end{bmatrix} \kappa \tag{5}$$

where J_b corresponds to the second moment of inertia of the beam cross-section. The damping torque T_d corresponds to

$$T_d = \begin{bmatrix} \sqrt{\frac{2G_b\ J_b}{l_0} I_r} & & \\ & \sqrt{\frac{E_b J_b}{l_0} I_r} & \\ & & \sqrt{\frac{E_b J_b}{l_0} I_r} \end{bmatrix} \Omega_{rel} \tag{6}$$

with the initial bond length l_0 and the reduced moment of inertia I_r, which is calculated from the individual moments of inertia of the particles connected with the bond according to

$$I_r = \frac{I_1 I_2}{I_1 + I_2} \tag{7}$$

For the calculation of all above-mentioned quantities, a circular bond cross-section is assumed. According to the beam theory, the stresses can be calculated on the basis of the strain and curvature of the bond element

$$\sigma_{s,ax} = \begin{bmatrix} E_b & & \\ & G_b & \\ & & G_b \end{bmatrix} \Gamma \tag{8}$$

$$\sigma_{t,b} = \begin{bmatrix} G_b & & \\ & E_b & \\ & & E_b \end{bmatrix} \kappa r_b \tag{9}$$

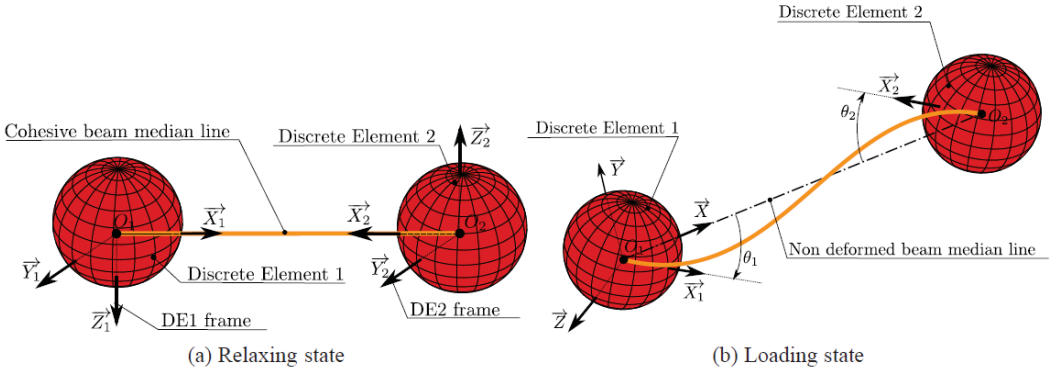

(a) Relaxing state (b) Loading state

Fig. 1 Bond element connecting two particles in its initial state (a) and in the loaded state (b) [18]

where r_b corresponds to the radius of the bond.

The equivalent stress is calculated using the von Mises yield criterion (cf. (10)). It should be noted that due to the material being much more sensitive to tensile stress, the normal stress component is only considered under tension and not under compression.

$$\sigma_v = \sqrt{{\sigma_{axial}}^2 + 3{\tau_{shear}}^2} \tag{10}$$

When a critical equivalent stress $\sigma_{v,krit}$ is reached, the bond is deleted, and the bonded particles experience no additional reaction forces based on this slave contact model henceforth. Due to the forces and moments being expressed in a local bond coordinate system, a final transformation into global coordinates is required.

III. Sample Generation

The sub-particles are modeled as spheres, which allows a combination of suitable simulation results with a computationally efficient simulation, and also a fast generation of the complex-shaped parent particles. The generation process follows a simple scheme: A three-dimensional volume is filled with sub-particles, which are then bonded together. This procedure can easily be simulated in a DEM software, if the required shapes of the parent particles are simple, as do the calibration samples in this paper as well as the filter cake plates generated for future simulations. Although this method of generating breakable parent particles may appear to be the easiest at first glance, it quickly reaches its limits if more complex geometries are required. Furthermore, the computational effort for simulating the filling process increases exponentially with increasing particle number, as usual for DEM simulations.

Another generation method, which requires a one-time preparation effort, is the use of a filling algorithm, of which several already exist, both for arbitrarily shaped sub-particles [19] as well as for spherical ones. In this project, a filling algorithm was implemented in which three adjacent spherical sub-particles are initially placed in a seed within an arbitrary geometry given by a triangulated surface mesh, following the placement of additional sub-particles as close as possible to the already generated particles following a desired particle size distribution (PSD) [20]. As a result, the volume of the parent particle is filled with adjacent particles starting from the seed until the to be added sub-particles collide with the surface mesh, as can be exemplarily seen in in Fig. 2. During the filling process, each newly placed particle is directly bonded to its immediate neighbor resulting in a bonding network shown in Fig. 2 (e). The generated parent-particle consists of 41,788 sub-particles and 235 220 bonds.

Depending on the material, care must be taken not to introduce any preferred crack paths [21] into the parent particle during generation, which can be easily controlled when using a filling algorithm. In addition to a much shorter generation time of the parent particle by means of a filling algorithm, compared with the simulation of the filling process, an algorithm is also characterized by the fact that the computation time increases significantly slower with increasing particle number.

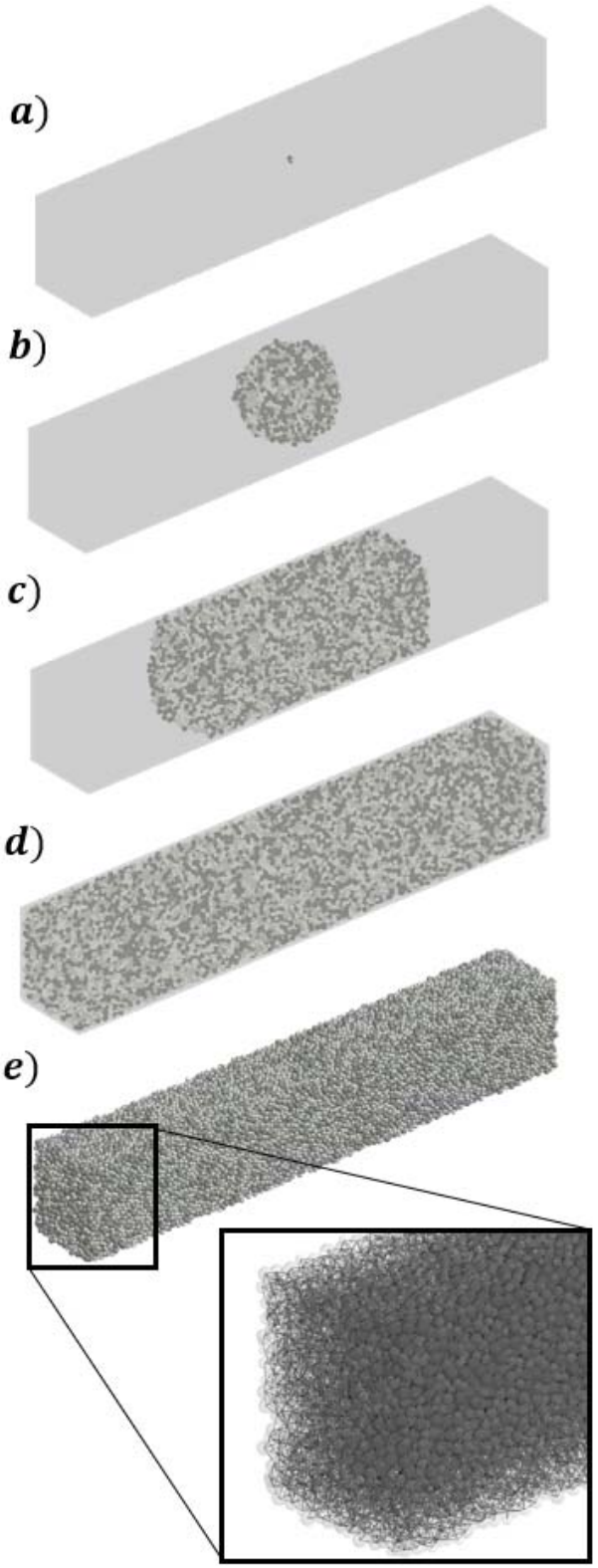

Fig. 2 Visualization of the sample generation using a filling algorithm starting with a seed within the desired geometry specified by an STL file (a), the filling process (b)-(d) and the finished parent particle within the DEM software including a closeup of the bonds connecting the sub-particles (e)

IV. Calibration Test

To obtain results from the simulation of a process in a suitable form, meaning the depiction of the correct macroscopic behaviour,the simulation micro parameters must be sufficiently calibrated. For this purpose, suitable calibration tests, i.e. reflecting the loads prevailing in the final process, must be selected. The calibration of typical simulation parameters, such as particle density or friction coefficients between particles, is not further discussed in this paper, since values in these contexts can be determined with commonly-known, standardized tests, such as an angle of repose test (cf. [22]).

For the calibration of rock and rock-like materials, whereby rock-like materials are understood to be materials that exhibit the same failure criteria as rock and, above all, brittle material behavior [23], numerous standardized tests already exist. These tests are used to determine characteristic material parameters, such as tensile or compressive strength. Due to the tensile strength of the filter cake being significantly lower than the compressive strength, as is common for rock-like materials, and the parent particles being initialized in thin plates in the final simulation, resulting the parent particle to most likely fail due to bending, i.e. due to tensile stress in the edge fiber, standardized tests that measure tensile strength are chosen to calibrate the bond parameters. Thus, the four-point bending flexural test is considered since it is not only used to measure tensile strength but also leads to material failure due to bending. The three-point bending flexural test is not considered in detail due to its dependence of the results on the specimen shape [24].

The procedure of the four-point bending flexural test, as well as the sample dimensions, are specified in various international standards for testing rock or cement-based products (e.g. EN 13161, ASTM C880-89). Since, in this application, the height of the specimen is specified by the filter press, a slightly modified sample geometry and position of the force application are selected. In the laboratory test, the sample is loaded with a force F divided between two loading points, as can be seen in Fig. 3 (a), to subject the specimen to a constant bending moment and no shear forces between those points. The force F is increased continuously to ensure a constant deformation rate v of 0.0002 m/s until the material failure occurs under the maximum force F_{max} at a deformation of $w_{s,max}$ depicted in Fig. 3 (b), while measuring the applied forces as well as the deformation.

The length L_S of the test sample was set at 180 mm, the width b_S at 30 mm, the sample thickness h_S given by the filter press is 35 mm and the distance between the loading points d_S at 80 mm. The resulting mean μ of the measured values as well as the standard deviation σ of several tests are shown in Fig. 4.

To calibrate the parameters of the bonds, the laboratory test is replicated in the simulation environment with the parent-particle being deformed at the same rate until failure occurs. A comparison of the laboratory test with the simulation results is shown in Fig. 5, where in this case, the broken bonds are highlighted instead of deleted to better visualize the fracture of the simulated test sample. Subsequently, the deformation path of the simulated sample as well as the required force are compared with the values measured in the laboratory tests, see Fig. 6.

When comparing the results of the laboratory tests and the simulation, it can be seen that the failure occurs at the same force and deformation. Due to averaging several laboratory tests, the curves deviate from each other. However, since these local deviations are marginal and the material limit state is depicted accurately this is considered negligible.

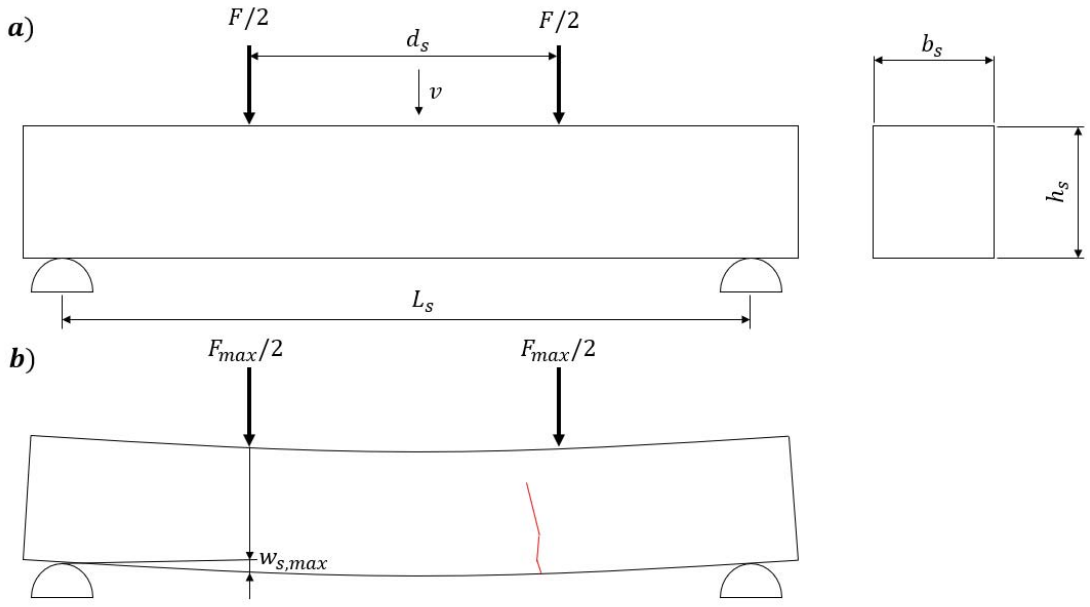

Fig. 3 Schematics of the four-point bending flexural test, showing the beginning of the experiment (a) and the breaking of the test sample (b)

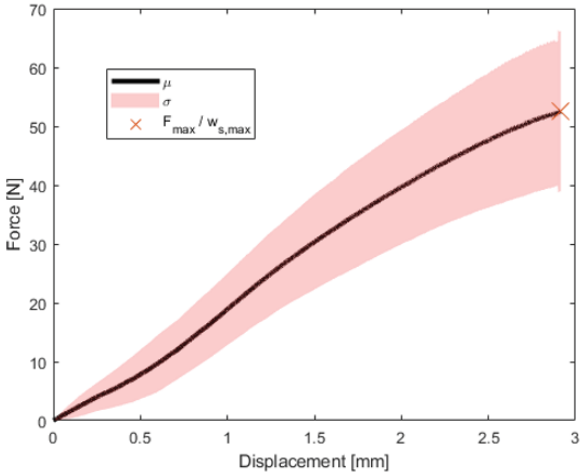

Fig. 4 Mean and standard deviation of the measured force over the displacement

V. Simulation Parameters

To ensure an efficient calibration of the simulation model, the parameters with the most significant influence on the simulation results are determined. These parameters are both general simulation parameters, such as the timestep and particle size, as well as model-specific micro-parameters.

1) Timestep: The timestep (Δt) has a great influence on a DEM simulation since its size affects the computational efficiency as well as the stability and accuracy of the simulation. For this reason, it should be chosen as large as possible but not to exceed a critical value at which the simulation tends to become unstable. Influenced by several different simulation parameters, this critical value also depends on the type of interaction.

For particle-particle interactions or particle interacting with system components, about 20% of the Rayleigh timestep $t_{Rayleigh}$ [25] is usually used to determine a suitable timestep, which corresponds to

$$t_{Rayleigh} = \frac{\pi \ R \ \sqrt{\frac{\rho}{G}}}{0.1631 \ \upsilon + 0.8766} \tag{11}$$

with the particle Radius R, density ρ, shear modulus G and Poisson's ratio υ, all being constant for all particles except the Radius, resulting in the critical timestep being that of the smallest particle Radius.

For bonded structures the critical value is calculated from the critical vibration frequency of the particles connected with massless bonds [26], following

$$t_{Bond,crit.} = 0.17\sqrt{\frac{m}{K}} \tag{12}$$

in three-dimensional space, with the particle mass m and bond stiffness K. This value is determined for the smallest, and therefore the lightest, particles bonded together with the highest bond stiffness. The timestep used in the simulation is the smallest critical timestep calculated from bonded and non-bonded contacts.

$$\Delta t = min(t_{Rayleigh}; t_{Bond,crit.}) \tag{13}$$

2) Bond Stiffness: The stiffness of the bonds corresponds to the macroscopic Youngs Modulus, which can be measured by means of local instrumentation during the calibration tests. In this case, the material's Youngs Modulus E is calculated from the beam deformation w_s at a loading point under a load F according to the elastic beam theory

$$w_s = \frac{F}{48 \ E \ I} \ (L_S - d_S)^2 \ (L_S + 2 \ d_S) \tag{14}$$

with the second moment of area I of the sample cross-section. By transforming this equation and applying the average values resulting from the experiments performed (the values for deformation and force at which material failure occurs, $w_{s,max}$ and F_{max}), the macroscopic Young's modulus is calculated, resulting in 13.2 MPa.

It is most convenient to initially deactivate the ability of the bonds to break when calibrating the bond's stiffness. The lower the stiffness of the bonds, the less force must be applied to deform the parent-particle to achieve the desired state of deformation. If a lower force at the deformation at which the fracture occurs in the laboratory test is measured in the simulation with the bond stiffness set as the macroscopic Youngs Modulus, the stiffness is continuously increased until the exact laboratory values are reproduced, respectively decreased if a higher force is measured.

3) Critical Stress: In order to reproduce the results of the laboratory tests, the maximum bond tensile stress at the desired fracture point is evaluated from the calibration simulation, which is then checked and fine-tuned, if necessary, in subsequent simulations. In addition to this, the results can be checked for plausibility by calculating the tensile stress due to the bending moment according to (15).

$$\sigma_b = \frac{3F(L_S - d_S)}{2 \ b_S {h_S}^2} \tag{15}$$

4) Sub-particle Size: Although the size of the sub-particles is not considered a classic simulation parameter, it has a considerable influence on the results of the calibration simulation. That is why the relation between the smallest distance within the sample geometry L to the average sub-particle diameter d must be taken into account when establishing the PSD used in the simulation. When testing the compressive strength of Rock the American Society for Testing and Materials (ASTM) recommends a ratio of L to the maximum grain size d_{max} of 10, while the International Society for Rock Mechanics (ISRM) suggests this ratio to be at least 20. When applied to DEM modeling, a ratio of L/d of 25 is recommended to keep the coefficient of variation of most model parameters under 2% [28].

VI. Conclusion

Complex-shaped particles capable of breaking are encountered in a wide range of technical processes, which are

consequently often to be analyzed via numerical simulations using the DEM. In this paper, a computationally-efficient filling algorithm was used to generate arbitrarily shaped parent-particles composed of sub-particles, which are

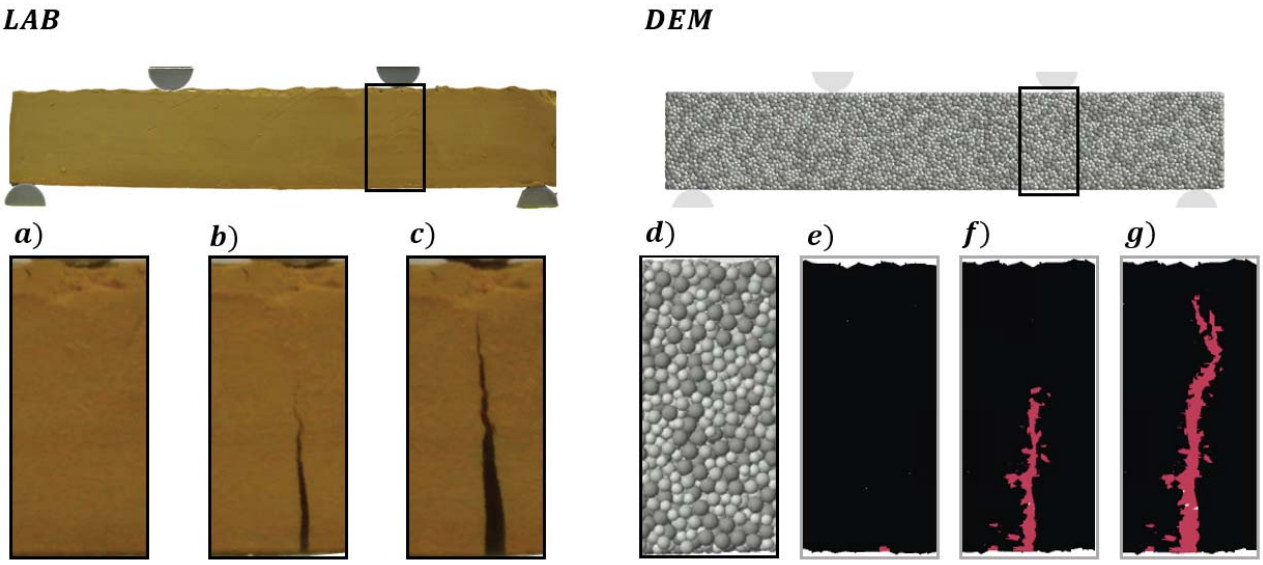

Fig. 5 Visual comparison of the material failure in the calibration test (LAB) and the simulation (DEM) under the maximum force F_{max}. Closeup of test sample (a) and crack propagation (b) and (c), as well as closeup of the simulated parent-pacticle with the sub-particles visible at first (d), then depicting a cross-section with only the bonds visualized (e) and finally the crack propagation (f) and (g) with the broken bonds highlighted

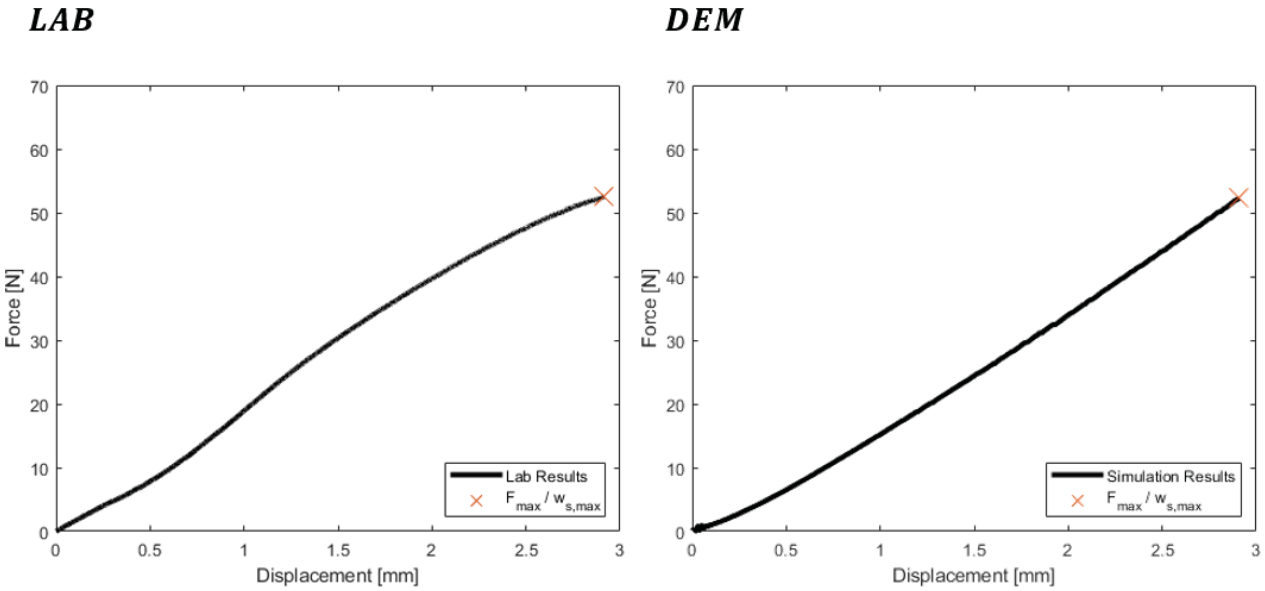

Fig. 6 Comparison of the measured data from the laboratory tests (LAB) and the simulation environment (DEM)

TABLE I
SUMMARY OFT THE DEM SIMULATION PARAMETER

Property	Describtion	Value	
ρ	Particle density	3 720	[kg/m³]
G	Particle Shear modulus (reduced, as typicall; cf [27])	10	[MPa]
μ	Particle interaction friction coefficient	0.67	[-]
d_{min}	Minimum Particle diameter	0.7	[mm]
d_{max}/ d_{min}	Ratio of maximum to minimum particle diameter	1.43	[-]
L/d	Ratio of characteristic length of the parent particle to median particle diameter	35	[-]
Eb	Bond Youngs Modulus	12.8	[MPa]
$\sigma_{v,krit}$	Critical equivalent bond stress	0.24	[MPa]

furthermore connected with deformable beams, termed bonds. An efficient way to choose the general simulation parameters as well as to calibrate the Bonded Particle Model parameters was shown by means of a four-point bending flexural test. This allows an easy way of generating, calibrating, and consequently simulating complex-shaped, deformable, and furthermore breakable bodies representing a brittle, rock-like material behavior in an efficient and suitable form to depict relatively large amounts of bulk media containing such complex types of DEM particles.

VII. Outlook

In order to simulate industrial-sized processes with several differently shaped parent-particles, further aspects have to be taken into consideration. Besides maintaining a realistic mass and volume flow during the breakage process, the optimization in regard to computational efficiency, as well as the consideration of the dynamic behavior of the parent-particles, the possibility to automatically detect different sub-particle clusters resulting from the breakage of bonded particle structures is of great interest.

References

[1] Michael Denzel and Michael Prenner. "Minimierung des Sinterzerfalls mittels DEM". In: *BHM Berg- und Hüttenmännische Monatshefte* 166.2 (2021), pp. 76–81. ISSN: 0005-8912. DOI: 10.1007/s00501-021-01081-7.

[2] Eugenio Oñate et al. "A local constitutive model for the discrete element method. Application to geomaterials and concrete". In: *Computational Particle Mechanics* 2.2 (2015), pp. 139–160. ISSN: 2196-4378. DOI: 10.1007/s40571-015-0044-9.

[3] Peter Domone and Marios Soutsos, eds. *Construction materials: Their nature and behaviour*. 5. ed. Boca Raton: CRC Press, Taylor & Francis Group, 2018. ISBN: 1315164590.

[4] Zong-Xian Zhang. *Rock Mechanics Related to Mining Engineering*. Helsinki, Finland, October 11–12, 2017.

[5] Peixian Li, Lili Yan, and Dehua Yao. "Study of Tunnel Damage Caused by Underground Mining Deformation: Calculation, Analysis, and Reinforcement". In: *Advances in Civil Engineering* 2019 (2019), pp. 1–18. ISSN: 1687-8086. DOI: 10.1155/2019/4865161.

[6] Johannes Quist and Carl Magnus Evertsson. "Cone crusher modelling and simulation using DEM". In: *Minerals Engineering* 85 (2016), pp. 92–105. ISSN: 08926875. DOI: 10.1016/j.mineng.2015.11.004.

[7] R. A. Bearman, C. A. Briggs, and T. Kojovic. "The applications of rock mechanics parameters to the prediction of comminution behaviour". In: *Minerals Engineering* 10.3 (1997), pp. 255–264. ISSN: 08926875. DOI: 10.1016/S0892-6875(97)00002-2.

[8] Martin Obermayr et al. "A bonded-particle model for cemented sand". In: *Computers and Geotechnics* 49 (2013), pp. 299–313. ISSN: 0266352X. DOI: 10.1016/j.compgeo.2012.09.001.

[9] Petre Miu. *Combine Harvesters: Theory, modeling, and design*. Boca Raton: CRC Press, 2015. ISBN: 9780429152931. DOI: 10.1201/b18852. URL: https://www.taylorfrancis.com/books/9781482282375.

[10] Qirui Wang, Hanping Mao, and Qinglin Li. "Modelling and simulation of the grain threshing process based on the discrete element method". In: *Computers and Electronics in Agriculture* 178 (2020), p. 105790. ISSN: 01681699. DOI: 10.1016/j.compag.2020.105790.

[11] Todd Wisdom, Mike Jacobs, and James Chaponnel. "GeoWasteTM – continuous comingled tailings for large-scale mines". In: *Proceedings of the 21st International Seminar on Paste and Thickened Tailings*. Proceedings of the International Seminar on Paste and Thickened Tailings. Australian Centre for Geomechanics, Perth, 2018, pp. 465–472. DOI: 10.36487/ACG_rep/1805_38_Wisdom.

[12] P. A. Cundall and O. D. L. Strack. "Discussion: A discrete numerical model for granular assemblies". In: *Géotechnique* 30.3 (1980), pp. 331–336. ISSN: 0016-8505. DOI: 10.1680/geot.1980.30.3.331.

[13] John A. Hudson, ed. *Comprehensive rock engineering: Principles, practice & projects*. 1. ed. Oxford [u.a.]: Pergamon Press, 1993. ISBN: 9780080406152.

[14] Nicholas J. Brown, Jian-Fei Chen, and Jin Y. Ooi. "A bond model for DEM simulation of cementitious materials and deformable structures". In: *Granular Matter* 16.3 (2014), pp. 299–311. ISSN: 1434-5021. DOI: 10.1007/s10035-014-0494-4.

[15] Peter Wriggers and B. Avci. "Discrete Element Methods: Basics and Applications in Engineering". In: *Modeling in Engineering Using Innovative Numerical Methods for Solids and Fluids*. Ed. by Riva, Laura de Lorenzis, and Alexander Düster. Vol. 599. CISM International Centre for Mechanical Sciences. Cham: Springer International Publishing, 2020, pp. 1–30. ISBN: 978-3-030-37517-1. DOI: 10.1007/978-3-030-37518-8_1.

[16] *ThreeParticle/CAE*. URL: http://becker3d.com/.

[17] D. O. Potyondy and P. A. Cundall. "A bonded-particle model for rock". In: *International Journal of Rock Mechanics and Mining Sciences* 41.8 (2004), pp. 1329–1364. ISSN: 13651609. DOI: 10.1016/j.ijrmms.2004.09.011.

[18] Damien André et al. "Discrete element method to simulate continuous material by using the cohesive beam model". In: *Computer Methods in Applied Mechanics and Engineering* 213-216 (2012), pp. 113–125. ISSN: 00457825. DOI: 10.1016/j.cma.2011.12.002.

[19] Y. Ma et al. "Packing Irregular Objects in 3D Space via Hybrid Optimization". In: *Computer Graphics Forum* 37.5 (2018), pp. 49–59. ISSN: 01677055. DOI: 10.1111/cgf.13490.

[20] Elias Lozano et al. "An efficient algorithm to generate random sphere packs in arbitrary domains". In: *Computers & Mathematics with Applications* 71.8 (2016), pp. 1586–1601. ISSN: 08981221. DOI: 10.1016/j.camwa.2016.02.032.

[21] H. A. Carmona et al. "Fragmentation processes in impact of spheres". In: *Physical Review E* 77.5 Pt 1 (2008), p. 051302. ISSN: 1539-3755. DOI: 10.1103/PhysRevE.77.051302.

[22] C. J. Coetzee. "Review: Calibration of the discrete element method". In: *Powder Technology* 310 (2017), pp. 104–142. ISSN: 00325910. DOI: 10.1016/j.powtec.2017.01.015.

[23] Jinjin Ge and Ying Xu. "A Method for Making Transparent Hard Rock-Like Material and Its Application". In: *Advances in Materials Science and Engineering* 2019 (2019), pp. 1–14. ISSN: 1687-8434. DOI: 10.1155/2019/1274171.

[24] A. Coviello, R. Lagioia, and R. Nova. "On the Measurement of the Tensile Strength of Soft Rocks". In: *Rock Mechanics and Rock Engineering* 38.4 (2005), pp. 251–273. ISSN: 0723-2632. DOI: 10.1007/s00603-005-0054-7.

[25] Rayleigh. "On Waves Propagated along the Plane Surface of an Elastic Solid". In: *Proceedings of the London Mathematical Society* s1-17.1 (1885), pp. 4–11. ISSN: 00246115. DOI: 10.1112/plms/s1-17.1.4.

[26] Catherine O'Sullivan and Jonathan D. Bray. "Selecting a suitable time step for discrete element simulations that use the central difference time integration scheme". In: *Engineering Computations* 21.2/3/4 (2004), pp. 278–303. ISSN: 0264-4401. DOI: 10.1108/02644400410519794.

[27] Stef Lommen, Dingena Schott, and Gabriel Lodewijks. "DEM speedup: Stiffness effects on behavior of bulk material". In: *Particuology* 12 (2014), pp. 107–112. ISSN: 16742001. DOI: 10.1016/j.partic.2013.03.006.

[28] Xiaobin Ding et al. "Effect of Model Scale and Particle Size Distribution on PFC3D Simulation Results". In: *Rock Mechanics and Rock Engineering* 47.6 (2014), pp. 2139–2156. ISSN: 0723-2632. DOI: 10.1007/s00603-013-0533-1.